chemistry

MDPI

Article

An Extensive Study of the Production of Hydrogen by Cellulose and Lignin Pyrolysis Using Rhenium-Based Catalysts

Mizraim Guillermo Granados-Fitch [1], Juan Manuel Quintana-Melgoza [2], Erick Adrian Juarez-Arellano [3,*] and Miguel Avalos-Borja [1]

[1] Instituto Potosino de Investigación Científica y Tecnológica, División de Materiales Avanzados, Camino a la Presa San José, Col. Lomas, Sección 4, San Luis Potosí C.P. 78216, Mexico
[2] Facultad de Ciencias Químicas e Ingeniería, Universidad Autónoma de Baja California, Campus Tijuana, Tijuana C.P. 22424, Mexico
[3] Centro de Investigaciones Científicas, Instituto de Química Aplicada, Universidad del Papaloapan, Circuito central # 200, Col. Parque Industrial, Tuxtepec C.P. 68301, Mexico
* Correspondence: eajuarez@unpa.edu.mx; Tel.: +52-287-8759240

Abstract: The use of rhenium-based catalysts (Re_2C, Re_3B, ReB_2, and ReS_2) obtained by mechanosynthesis in the pyrolysis of cellulose and lignin from 500 to 800 °C using 10 and 20 wt.% of catalysts is reported. The mechanosynthesis of ReS_2 has been reported for the first time. The catalytic pyrolysis of cellulose resulted in maximum H_2 production at 800 °C and 10 wt.% catalyst, with 44% H_2 yield using a Re_3B catalyst. In contrast, lignin catalytic pyrolysis also showed maximum production under the same conditions, with an 86.1% H_2 yield using the NiO/SiO_2 catalyst; however, the catalyst did not drastically enhance H_2 production. H_2 formation by cellulose pyrolysis is a thermocatalytic process, whereas lignin pyrolysis is an entirely thermic process. A reaction mechanism was proposed to explain the H_2 formation by both catalytic cellulose and lignin pyrolysis.

Keywords: rhenium; carbide; boride; sulfide; hydrogen; pyrolysis; catalyst

check for updates

Academic Editor: Vasile I. Parvulescu

Received: 24 December 2024
Revised: 7 February 2025
Accepted: 24 February 2025
Published: 1 March 2025

Citation: Granados-Fitch, M.G.; Quintana-Melgoza, J.M.; Juarez-Arellano, E.A.; Avalos-Borja, M. An Extensive Study of the Production of Hydrogen by Cellulose and Lignin Pyrolysis Using Rhenium-Based Catalysts. *Chemistry* **2025**, *7*, 33. https://doi.org/10.3390/chemistry7020033

Copyright: © 2025 by the authors. Licensee MDPI, Basel, Switzerland. This article is an open access article distributed under the terms and conditions of the Creative Commons Attribution (CC BY) license (https://creativecommons.org/licenses/by/4.0/).

1. Introduction

The rise of civilization and national prosperity is possible through energy consumption. There are many different sources of energy supply, such as primary (directly consumed, e.g., petroleum, coal, and natural gas), secondary (used in refined form, e.g., gasoline, diesel, geothermal, and biomass), and tertiary (feature several transformations of energy, e.g., electric energy and nuclear energy) [1]. The most important primary energy sources that satisfy global energy demand in 2024 are oil (31.2%), coal (27.2%), natural gas (24.7%), renewables (e.g., biomass and waste, 6.9%), and nuclear energy (4.3%) [2]. Petroleum, coal, and natural gas are non-renewable energy sources, and their current rates of extraction and consumption tend to deplete rapidly. Alternative renewable energy sources such as solar energy, wind power, geothermal energy, power from water (e.g., hydroelectric, tidal, ocean currents, wave power), and biomass will reach USD 1512.3 billion in the global renewable energy market by 2025 [3].

Molecular hydrogen (H_2) is a clean and reliable energy carrier that can be used as an alternative to fossil fuels. The most significant advantage is the production of water via combustion with oxygen [4]. H_2 is produced worldwide from primary energy sources via four catalytic processes: steam methane reforming, partial oxidation of hydrocarbons, auto-thermal reforming, and coal gasification [5]. Biomass pyrolysis is a new process for H_2 production that has been studied extensively under non-catalytic and catalytic conditions.

Biomass is a complex mixture of three organic biopolymers: cellulose (40–50 wt.%), hemicellulose (20–40 wt.%), and lignin (5–30 wt.%) [6]. Biomass is abundant, and there have been many efforts worldwide to use it as a resource to generate alternative energy (fuels, electricity, heat, hydrogen, etc.). Although cellulose is widely used in various applications, lignin has been considerably sub-utilized. Therefore, this study focuses on these two main biomass components.

Regarding the production of H_2 from cellulose pyrolysis, the results were diverse under noncatalytic pyrolysis conditions. While Simmons et al. [7] reported that H_2 was not obtained, Wu et al. [8] reported up to 5.8 mmol H_2/g cellulose at 500 °C, whereas Lanza et al. [9] reported that the temperature rise during a short residence time increased the gas yield up to almost 100% at 900 °C. On the other hand, under catalytic pyrolysis conditions, the production of H_2 per gram of cellulose ranges from 0.19 to 773.28 mL of H_2 [10–23] depending on the catalyst and conditions used. Zhao et al. [10–12] reported up to 546 mL H_2 at 550 °C using a Ni-Co-CaO/SBA-15 catalyst, 527 mL H_2 at 550 °C using Ni-Co-CaO/SiO_2 and 773.28 mL H_2 at 450 °C using $Ca(OH)_2$:Ni. Widyaningrum et al. [13,14] reported 73.5 mL H_2 at 800 °C using 5Ni/MCF and 85 mL H_2 at 800 °C using 5Ni-0.7Pd/MCF. Matras et al. [15] reported 246.55 mL H_2 at 700 °C using 20Ni/ZrO_2. Ruppert et al. [16] reported 242.1 mL H_2 at 700 °C using NiO. Donar et al. [17] reported 56 mL H_2 at 700 °C using a 5% SnO_2 catalyst. Grams et al. [18–20] reported 349.66 mL H_2 at 700 °C using 20Ni/15CeO_2-ZrO_2, 237.59 mL H_2 at 700 °C using 20Ni/SBA-15 and 264.49 mL H_2 at 700 °C using a Ni/ZrAlSBA-15 catalyst. Ryczkowski et al. [21,22] reported 381.04 mL H_2 at 700 °C using 20Ni1Ca/ZrO_2 and 349.66 mL H_2 at 700 °C using 20Ni10CaO/ZrO_2, while Memon et al. [23] reported 0.19 mL H_2 at 800 °C using $NaZrO_3$ catalyst.

In the same way as for cellulose, the production of H_2 from lignin pyrolysis has been widely studied under noncatalytic and catalytic conditions. Under non-catalytic pyrolysis conditions, the main variables are temperature and heating rates [24–32]. Ferdous et al. [24,25] reported that H_2 production reached up to 73% yield at 800 °C using a heating rate of 15 °C/min. Baunlin et al. [26] reported 40% yield at 527 °C when kraft lignin was pyrolyzed. Widyawati et al. [27] reported that H_2 production occurs between 500 and 900 °C with a maximum at 750 °C. Wu et al. [8] reported the production of 40.32 mL of H_2 per gram of lignin at 500 °C. Zhou et al. [29] reported 172 mL H_2 at 900 °C. Akubo et al. [32] reported 156.8 mL H_2 at 550 °C.

Several studies have been conducted under catalytic pyrolysis conditions, and the production of H_2 per gram of lignin ranges from 11.2 to 682 mL of H_2 [33–36] depending on the catalyst and conditions used. Collard et al. [34] reported 47 mL H_2 at 800 °C using a nickel salt catalyst. Milovanovic et al. [35] reported 682 mL H_2 at 500 °C using NiO/H-Y. Yang et al. [36] reported 11.2 mL H_2 at 650 °C using a HZSM-5 catalyst.

Therefore, previous studies on cellulose and lignin pyrolysis have shown that the most important parameters for H_2 production are high temperature and the amount of catalyst used. However, not every catalyst can be used at high temperatures because of its low melting point or low sintering temperature (microstructural changes that affect the catalytic activity). Thus, rhenium-based catalysts were proposed in this study. Rhenium and rhenium-based catalysts have already been used to produce H_2 [37–39]. They are of great interest because of their outstanding properties, such as heat resistance, high melting point, high density, and extraordinary corrosion resistance. In this study, rhenium-based catalysts (Re_2C, Re_3B, ReB_2, and ReS_2) obtained by mechanosynthesis were tested for H_2 production from cellulose and lignin pyrolysis. The mechanosynthesis of ReS_2 and its use as a catalyst in the production of H_2 have been reported for the first time. Pyrolysis was performed from 500 °C to 800 °C using 10 and 20 wt.% of catalyst. Thus, this study aimed to identify the best temperature and weight percentage of the catalyst to maximize H_2

production from both cellulose and lignin pyrolysis. In addition, heteroatoms (C, B, and S) had an effect on the catalytic activity and proposed a reaction mechanism for both the cellulose and lignin catalytic pyrolysis processes.

2. Materials and Methods

2.1. Raw Material and Chemicals

Rhenium (Re, 99.95% purity) and 60%NiO/SiO_2 commercial catalyst (labeled as NiO/SiO_2 catalyst) were acquired from Merck (Merck S.A. de C.V., Naucalpan de JuárezEstado de Mexico, Mexico). Sulfur (S, 99.8%, sublimed, Fermont) was acquired from Reactivos y Equipos S.A. de C.V. (San Pedro Garza García, Nuevo Leon, Mexico). Cellulose (powder, α-cellulose) and lignin (powder, alkaline, average MW~10,000, 4 wt.% S) were also acquired from Merck.

2.2. Mechanosynthesis and Characterization of Rhenium-Based Catalysts

The mechanosynthesis and the appropriate characterization of all other catalysts (Re_2C, Re_3B, and ReB_2) were reported in detail elsewhere (Re_2C catalyst [38,40] and rhenium boride catalysts (Re_3B and ReB_2) [39–41]).

Rhenium forms two sulfides, rhenium (IV) sulfide (ReS_2) and rhenium (VII) sulfide (Re_2S_7). ReS_2 is a semiconductor with a bandgap of approximately 1.4 eV. It has been synthesized using a variety of methods, including chemical vapor transport from rhenium and sulfur [42], rhenium sulfidation [43], chemical vapor deposition [44], thermal decomposition of molecular complexes [45], and chemical reactions from inorganic precursors [46]. However, mechanochemical synthesis of ReS_2 has not yet been reported.

The ReS_2 synthesis was carried out as follows. Briefly, a 1:2 elemental ratio mixture of rhenium and sulfur with a final weight of 5 g was mechanically treated with a mortar and pestle until a homogenous powder was obtained. A WC grinding vial (55 mL volume) with the mixture and 10 balls of WC (11.2 mm in diameter) were placed in a 8000 Mixer/mill (SPEX SamplePrep, Metuchen, NJ, USA), and milling was carried out and monitored every 400 min of milling time by XRD using a Rigaku SmartLab diffractometer (Rigaku, Cedar Park, TX, USA). The surface area was obtained by the BET method using an ASAP 2020 Micromeritics (The Micromeritics Instrument Corporation, Norcross, GA, USA) accelerated surface area system. The morphology and microstructure were characterized using scanning electron microscopy (SEM, Helios Nanolab 600) (Thermo Fisher Scientific, Waltham, MA, USA) and transmission electron microscopy (TEM, Tecnai F30) (Thermo Fisher Scientific, Waltham, MA, USA).

2.3. Cellulose and Lignin Pyrolysis Using Rhenium-Based Catalysts

Cellulose and lignin catalytic pyrolysis were evaluated through the production of H_2, CH_4, CO, and char generation. The pyrolysis was performed using a methodology reported elsewhere [37,38]. The pyrolysis system used in this study is shown in Figure S1. In summary, 100 mg of cellulose or lignin was placed in porcelain canoes with 10 and 20 wt.% of every rhenium-based catalyst (Re_2C, Re_3B, ReB_2, and ReS_2) and NiO/SiO_2 commercial catalyst. The canoe was placed inside a quartz tube in a Lindberg/Blue M Mini-Mite) (Thermo Fisher Scientific, Waltham, MA, USA). The carrier gas flow rate was 15 mL/min (helium, 99.998% purity). Catalytic pyrolysis was performed from 500 to 800 °C, and gaseous products were collected in a 10 L gasbag for 40 min in each experiment.

2.4. Monitoring of H_2, CH_4, CO Production and Char Waste Generation

The methodology used has been reported in detail elsewhere [37,38]. The monitoring system of H_2, CH_4, CO production used in this study is shown in Figure S2. In summary,

H_2, CH_4, and CO were measured using an 8610C gas chromatograph equipped with a TCD detector (SRI Instruments, Torrance, CA, USA) and a Washed MolSieve 5A packed column (Agilent Technologies Manufacturing GmbH & Co. KG, Waldbronn, Germany). The temperatures of the oven and detector were set to 50 °C and 120 °C, respectively. The standard external method was used to calibrate the gas chromatograph with a standard gas mixture of H_2, CH_4, and CO (1% of each component equivalent to 10,000 ppm, Supelco) to obtain the concentration of each component in the gasbag.

The concentration of each component of the gaseous products from CS pyrolysis can be calculated using Equation (1):

$$\text{ppm } (H_2, CH_4 \text{ or CO}) = S_Z/S_Y \times 10{,}000 \text{ ppm} \quad (1)$$

where S_Z is the peak area of each component in the gasbag and S_Y is the peak area of the corresponding components of the standard gas.

Char conversion is an important parameter to evaluate the total pyrolysis of biomass. The char of the pyrolysis of CS can be calculated using Equation (2):

$$\text{Char (mg)} = W_Z - W_Y \quad (2)$$

where W_Z is the weight of the carbonaceous residue after the pyrolysis of CS and W_Y is the weight of the catalyst used in each experiment.

3. Results and Discussion

3.1. Characterization of Catalysts

The mechanosynthesis of ReS_2 from the Re:S 1:2 stoichiometry was monitored using XRD, and the results are shown in Figure 1. The diffractogram at 100 min shows diffraction peaks of rhenium (▲, PDF4+ 01-087-0599) and sulfur (*, PDF4+ 01-074-1465). At 1600 min of milling time, a diffraction peak at 14.59 of 2θ is observed; this peak belongs to the most intense reflection, the (002) plane of the ReS_2 triclinic phase (♣, PDF4+ 04-007-2320). Based on the (002) FWHM peak and using the Scherrer equation, the crystallite size of the Re_2S particles was calculated to be approximately 3.7 nm. To our knowledge, this is the first report of the mechanosynthesis of ReS_2. However, at 2000 min of milling time, the diffractogram shows only peaks of unreacted rhenium and WC from the milling media (■, PDF4+ 04-007-5192). The disappearance of the (002) peak of ReS_2 from the 1600 to 2000 milling time diffractograms is principally attributed to the loss of crystallinity and the crystallite size reduction due to the mechanochemical energy transferred. It has been reported that crystallite sizes less than 3 nm cannot be detected by XRD [47].

Figure 2a shows the adsorption isotherm of the ReS_2 material after 2000 min of milling; it is of type III, where the interactions of the adsorbate play a significant role. The surface area of ReS_2 was 41.79 m^2g^{-1}. The SEM micrograph shows nanoparticles with an average size of less than 200 nm (Figure 2b), whereas the TEM micrograph shows a conglomerate of nanoparticles smaller than 100 nm (Figure 2c). Figure 2d shows that the conglomerate was integrated with the WC and ReS_2 nanoparticles. Figure 2d shows nanoparticles with interplanar distances of 0.63–0.67 nm, which are in good agreement with the value of 0.60 nm of the (002) plane of ReS_2 (PDF4+ 04-007-2320), confirming the formation of ReS_2 particles.

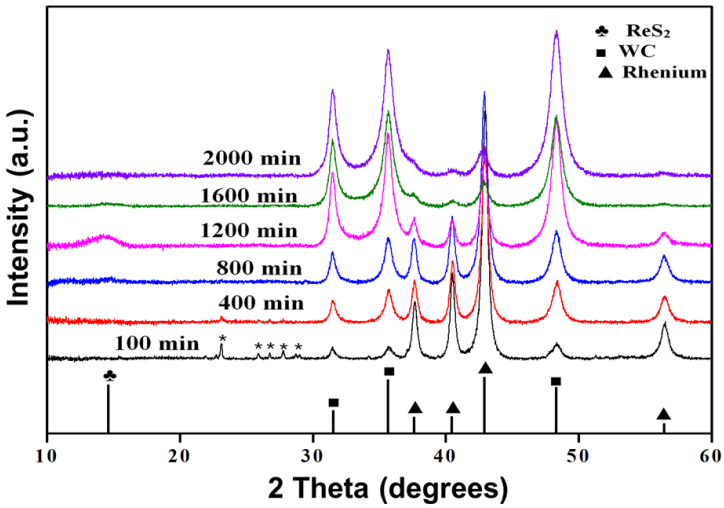


Figure 1. X-ray diffraction patterns of ReS_2 mechanosynthesis at different milling times. Crystallographic PDF4+ cards: rhenium (▲, 01-087-0599), tungsten carbide (■, 04-007-5192) and ReS_2 (♣, 04-007-2320). Sulfur (*, 01-074-1465).

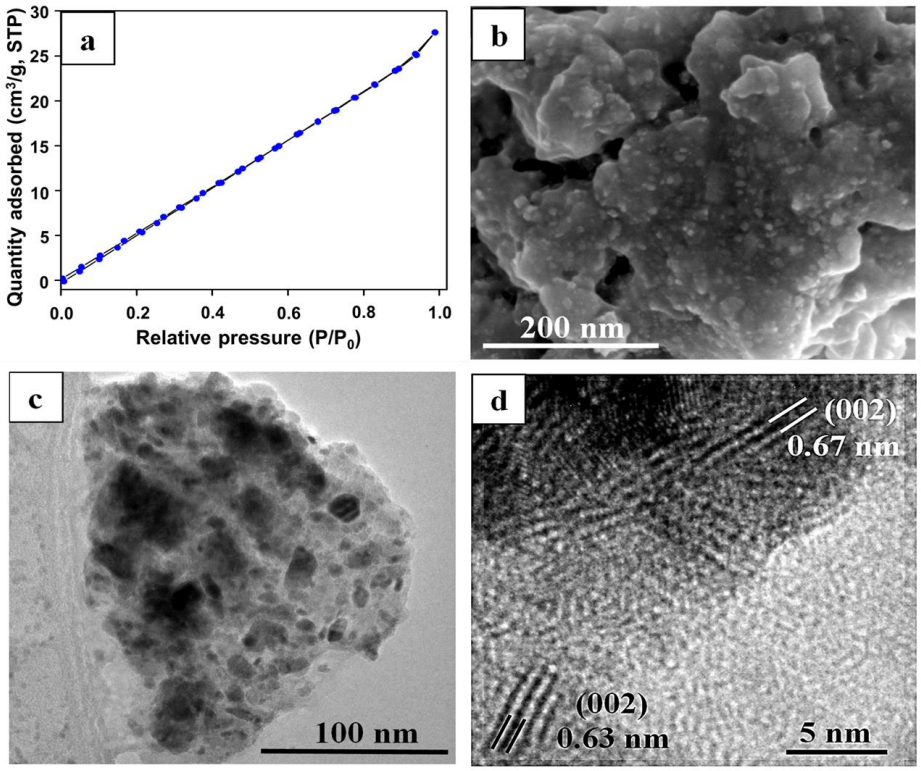


Figure 2. Surface and morphological characterization of the ReS_2 catalyst after 2000 min of milling. (**a**) BET isotherm and (**b**) SEM characterization. TEM bright field (**c**) and filtered image (**d**); the interplanar distances of 0.63 and 0.67 nm are in good agreement with the value of 0.60 nm belonging to (002) plane of ReS_2 (PDF4+ 04-007-2320).

Figure 3 shows the diffractogram of a NiO/SiO_2 commercial catalyst. It shows only diffraction peaks associated with NiO (PDF4+ 00-004-0835). No diffraction peaks corresponding to the SiO_2 phase were observed, which indicates an amorphous state.

The adsorption isotherm of the NiO/SiO_2 catalyst is type IV, which is related to mesoporous materials (Figure 4a). An important characteristic of this isotherm is that it exhibits a hysteresis loop of type H1 associated with porous materials and a narrow pore size distribution. The surface area of NiO/SiO_2 was 189.35 m^2g^{-1}. SEM micrographs

show that in the NiO/SiO_2 catalyst, two types of morphologies were observed: polyhedral particles with a size of less than 1 μm and dendritic particles with embedded polyhedral particles (Figure 4b). TEM was performed to characterize both morphologies, and the results are shown in Figure 4c,d. The dendritic particles were amorphous and associated with SiO_2 (Figure 4c), while the polyhedral particles were the catalyst (Figure 4d). A magnified and filtered image from the yellow box shows an interplanar distance of 0.24 nm in identical correspondence with the value of 0.24 nm with the (111) plane of NiO PDF4+ 00-004-0835. Thus, the XRD, SEM, and TEM characterizations confirmed that the polyhedral particles were NiO, whereas the dendritic amorphous material was the SiO_2 support.

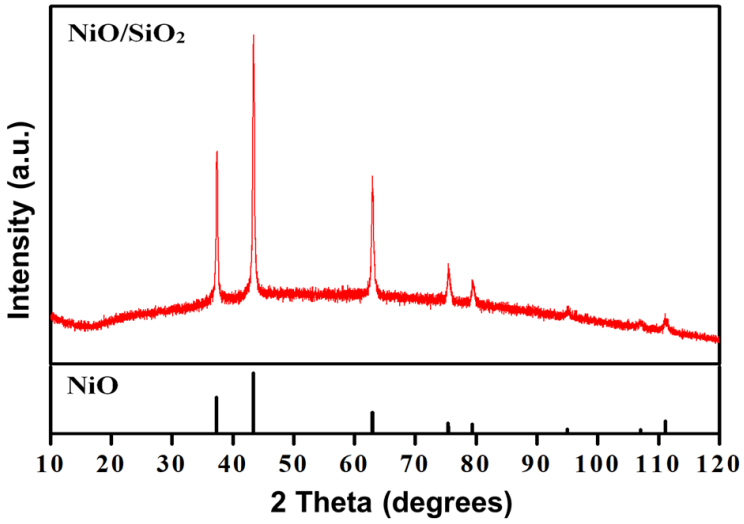


Figure 3. X-ray diffraction pattern of commercial catalyst NiO/SiO_2. Stick diagram of NiO, PDF4+ card 00-004-0835.

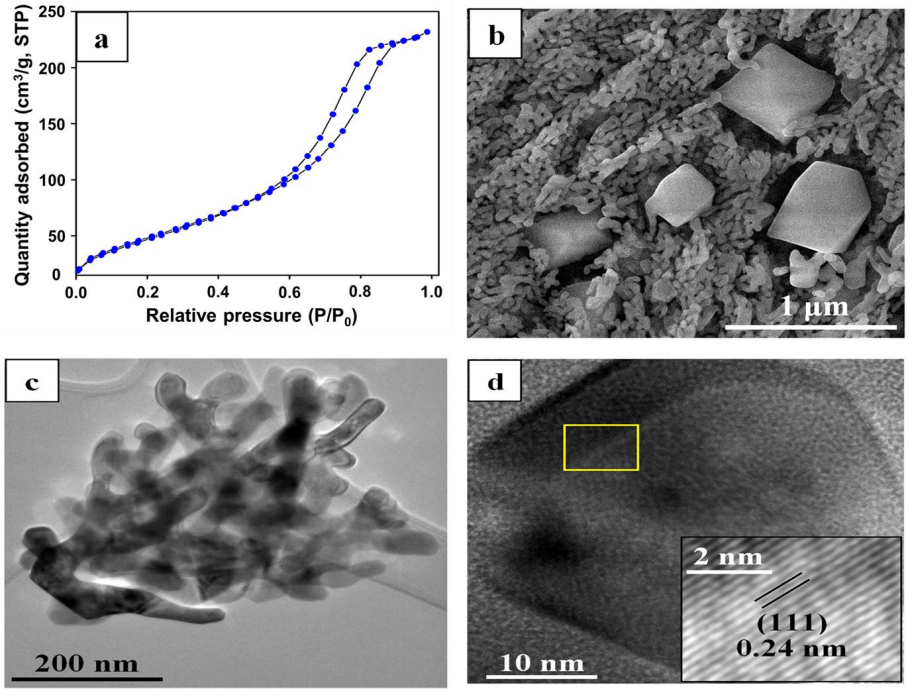


Figure 4. Surface and morphological characterization of the NiO/SiO_2 catalyst. (**a**) BET isotherm and (**b**) SEM characterization. TEM characterization (**c**,**d**); the interplanar distance of 0.24 nm in identical correspondence with the value of 0.24 nm of (111) plane of NiO PDF4+ 00-004-0835. The yellow rectangle in (**d**) shows the region where the high-resolution image shown at the bottom right of the image was obtained.

3.2. Cellulose Catalytic Pyrolysis

To evaluate the effect of rhenium-based catalysts on H_2, CH_4, and CO production and char generation, cellulose was pyrolyzed from 500 °C to 800 °C using 10 and 20 wt.% of Re_2C, Re_3B, ReB_2, ReS_2, and NiO/SiO_2 catalysts. The results are shown in Figures 5 and 6, and the values obtained at 800 °C are listed in Table 1. Figure 5a shows the H_2 production using 10 wt.% catalyst. The maximum H_2 production was observed using Re_3B, whereas the minimum was achieved without a catalyst (Table 1). Increasing the amount of the catalyst to 20 wt.% (Figure 5b), the same trend was observed. However, the results showed that 10 wt.% catalyst and 800 °C are the best conditions to maximize the H_2 production from cellulose catalytic pyrolysis since the gain observed when doubling the amount of catalyst is minimal. Only in the case of Re_2C did the H_2 production increase considerably, doubling the amount of the catalyst. Garnier et al. [48] reported that the H_2 content in cellulose is approximately 6.5 wt.% equivalent to 65,000 ppm of H_2. Taking this value as a reference, the H_2 yields achieved from cellulose pyrolysis at 800 °C in this study were 6.8% without the catalyst, 19.2% with ReS_2 (using 20 wt.% catalyst), 28.4% NiO/SiO_2 (10 wt.%), 30.7% ReB_2 (20 wt.%), 31.4% Re_2C (20 wt.%) and 44.0% Re_3B (10 wt.%).

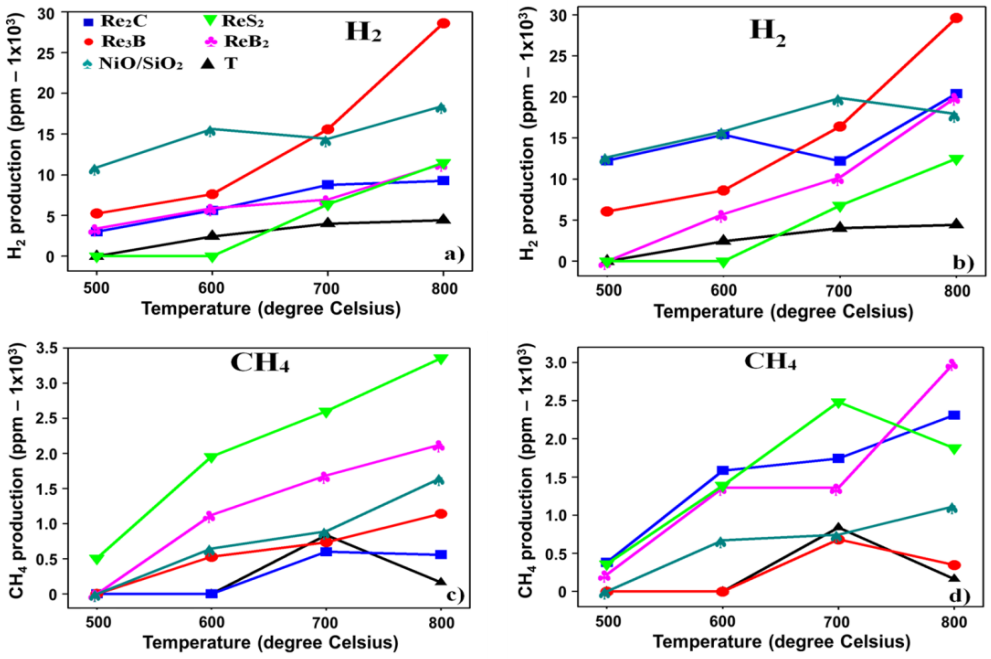


Figure 5. Catalytic pyrolysis of cellulose using rhenium catalysts. H_2 production: 10 wt.% (**a**) and 20 wt.% (**b**); CH_4 production: 10 wt.% (**c**) and 20 wt.% (**d**).

Table 1. The production of H_2, CH_4, CO, and char during the catalytic pyrolysis of cellulose at 800 °C using 10 and 20 wt.% rhenium-based catalysts.

Catalyst	10 wt.% Catalyst				20 wt.% Catalyst			
	H_2/ppm	CH_4/ppm	CO/ppm	Char/mg	H_2/ppm	CH_4/ppm	CO/ppm	Char/mg
without	4453	116	4453	8.7	4453	116	4453	8.7
ReS_2	11,512	3359	20,852	5.2	12,494	1880	32,587	2.1
ReB_2	11,389	2129	19,070	9.2	20,012	2298	28,182	9.1
Re_3B	28,616	1141	32,042	5.4	29,632	347	36,547	2.9
Re_2C	9272	557	8153	9.1	20,421	2312	19,613	8.9
NiO/SiO_2	18,486	1654	14,813	6.8	17,949	1120	17,802	3.1

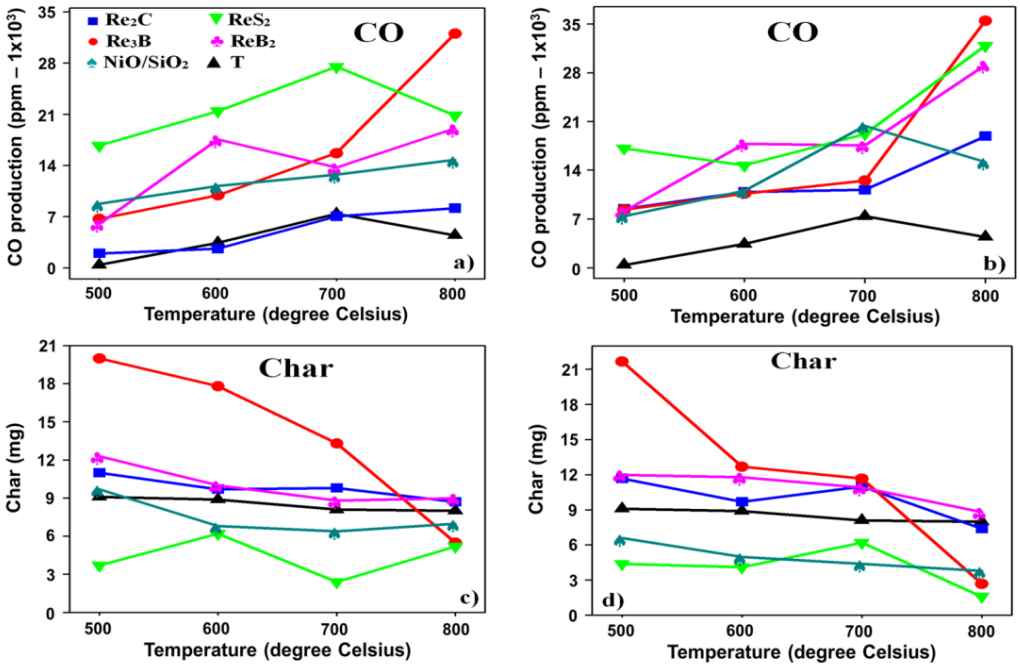


Figure 6. Catalytic pyrolysis of cellulose using rhenium catalysts. CO production: 10 wt.% (**a**) and 20 wt.% (**b**); char generation: 10 wt.% (**c**) and 20 wt.% (**d**).

Sabatier's principle [49] states that the key criterion in designing and screening electrocatalytic materials is that the binding energy between the catalyst and the reactant should be neither too strong nor too weak. To evaluate this principle, the adsorption energies of monoatomic H on C, B, S, Ni, and Re are listed in Table 2. From these energies, the absorption of hydrogen by Re from the Re_2C, Re_3B, ReB_2, and ReS_2 compounds indicated the formation of stable intermediate compounds, following Sabatier's principle [49]. Thus, it can be established that Re plays the principal role in these catalysts. However, the adsorption energy values for carbon allotropes are small; therefore, hydrogen adsorption by C in Re_2C creates an unstable intermediate compound with a negative effect on H_2 formation. Concerning hydrogen adsorption by B in Re_3B and ReB_2, the values were similar to those reported for Re. Ferro et al. [50,51] studied the interaction of hydrogen on the surface of boron-doped graphite. They found that the adsorption of two hydrogen atoms on adjacent B atoms causes them to spontaneously recombine to form molecular H_2 and that diffusion is the rate-limiting step. Therefore, the high% H_2 yield obtained using the Re_3B and ReB_2 catalysts is a combination of the positive effects of the Re and B active sites to form H_2. The higher% H_2 yield obtained using the Re_3B rather than the ReB_2 catalysts indicates that Re plays a more important role than B in these catalysts. In addition, the difference in the catalytic activity of B between Re_3B and ReB_2 is due to their oxidized surfaces, as shown by their TPR characterization reported elsewhere [39]. The values for hydrogen adsorption by S in ReS_2 are small. Therefore, hydrogen adsorption by S created an unstable intermediate compound with a negative effect on H_2 formation and hydrogen adsorption by C in Re_2C. In addition, the low% H_2 yield using the ReS_2 catalyst can be attributed to the formation of H_2S, as it has been reported that H_2S forms between 602 and 1290 °C [52]. Finally, the hydrogen adsorption by Ni in NiO/SiO_2 is like Re; therefore, it shows a high% H_2 yield.

Table 2. Adsorption energies of monoatomic hydrogen over the catalytic centers in the tested catalysts.

Process	Adsorption Energy (kJ mol^{-1})	Reference
Re-H	280, 272, 127, 125	[53–56]
C-H (CNT)	190, 185, 158	[57–59]
C-H (graphene)	140, 138, 73, 72, 66	[60–64]
C-H (graphite)	31	[65]
B-H	290, 144, 140	[66–68]
S-H	110 (PtS2), 103 y 63 (MoS2)	[69–71]
Ni-H	299, 200, 197	[72–74]

The results show that the Re_3B catalyst has the highest catalytic activity for H_2 production from cellulose pyrolysis, which is in good agreement with the results of H_2 production from coconut shell pyrolysis reported previously [38]. In addition, it was confirmed that rhenium catalysts increased H_2 production, promoting the dehydrogenation of H-C-O-H groups instead of the cellulose dehydration reaction [27].

The production of CH_4 using 10 wt.% is shown in Figure 5c. The maximum CH_4 production was observed using ReS_2, whereas the minimum was achieved without a catalyst (Table 1). Increasing the amount of catalyst to 20 wt.%, the same trend was observed (Figure 5d). However, the Re_3B catalyst had a negative effect on CH_4 formation, as the CH_4 production decreased from 1141 ppm (10 wt.%) to 347 ppm (20 wt.%). This result implies that the Re_3B catalyst has both the desired properties for use in H_2 production from biomass pyrolysis: high H_2 and low CH_4 production.

CO production using 10 wt.% of catalysts is shown in Figure 6a. The maximum CO production was observed using Re_3B, whereas the minimum was achieved without a catalyst (Table 1). Increasing the amount of catalyst to 20 wt.%, the same trend was observed (Figure 6b). The highest CO production was observed when the Re_3B catalyst was used, which was related to the highest H_2 production (Figure 5a) and lowest CH_4 production (Figure 5c). It has been reported that an increase in CO production positively affects H_2 formation [38,39]. Therefore, the Re_3B catalyst fulfills three essential functions for H_2 production from cellulose: high (H_2–CO) and low CH_4 production.

Char generation using 10 wt.% catalysts is shown in Figure 6a. The maximum char generation was observed using ReB_2, whereas the minimum was achieved using ReS_2 (Table 1). Increasing the amount of catalyst to 20 wt.%, the same trend was observed (Figure 6b). In all cases the char generation values are within 2.9–9.2 mg, which agrees with the values reported for char generation by cellulose pyrolysis (6.5 to 8.5 mg at 800 °C) [75–77].

To compare the results obtained in this study, Table 3 shows the H_2 production by cellulose pyrolysis using other methodologies. H_2 production from steam cellulose gasification was omitted because the H_2 yield was overestimated because of water decomposition. From the information in Table 3, several statements can be made about H_2 production by catalytic cellulose pyrolysis: (1) the catalytic pyrolysis of cellulose is a way to enhance H_2 production; (2) the surface area of the catalyst has a determinant role in the% H_2 yield; (3) the% H_2 yield of the Re_3B catalyst (44%) is one of the highest reported; (4) the high pyrolysis temperature, up to 800 °C, is vital to achieve a high H_2 yield; and (5) the recombination of monoatomic H to form H_2 is the most important step.

Table 3. H_2 yield by catalytic cellulose pyrolysis at high temperatures.

Catalyst	SBET (m^2g^{-1})	% H_2 Yield	Temperature	Reference
20Ni1Ca/ZrO_2	2.0	56.9	700 °C	[21]
20Ni10CaO/ZrO_2(CI) [a]	32.0	52.2	700 °C	[22]
20Ni10CaO/ZrO_2(I) [b]	37.0	50.2	700 °C	[22]
20Ni/ZrO_2	127.0	48.5	700 °C	[22]
20Ni/15CeO_2-ZrO_2(I) [b]	70.0	48.0	700 °C	[18]
20Ni1Na/ZrO_2	128.0	46.1	700 °C	[21]
20Ni/15CeO_2-ZrO_2(S) [c]	30.0	46.1	700 °C	[18]
20Ni1Mg/ZrO_2	7.0	45.5	700 °C	[21]
20Ni/50CeO_2-ZrO_2(I) [b]	47.0	44.9	700 °C	[18]
20Ni/50CeO_2-ZrO_2(S) [c]	9.0	44.9	700 °C	[18]
Re_3B	0.48	44.0	800 °C	This study
20Ni1K/ZrO_2	148.0	43.5	700 °C	[21]
20Ni/15CeO_2-ZrO_2(P) [c]	135.0	42.7	700 °C	[18]
20Ni/50CeO_2-ZrO_2(P) [c]	140.0	42.1	700 °C	[18]
Ni/ZrAlSBA-15 (I) [b]	495.0	40.1	700 °C	[20]
20Ni/ZrO_2	N.V.	37.4	700 °C	[15]
NiO	N.V.	36.8	700 °C	[16]
20Ni/ZrO_2	164.0	34.8	700 °C	[21]
20Ni/(10ZrO_2+Al_2O_3)	N.V.	33.4	700 °C	[15]
20Ni/SiO_2	N.V.	32.8	700 °C	[15]
20Ni/SBA-15	475.0	32.6	700 °C	[19]
Ni/SiO_2	219.0	32.4	700 °C	[20]
20Ni/KIT-6	397.0	32.0	700 °C	[19]
20Ni/CeO_2	N.V.	31.8	700 °C	[15]
20Ni/Al_2O_3	N.V.	31.4	700 °C	[15]
Re_2C	0.43	31.4	800 °C	This study
ReB_2	0.52	30.7	800 °C	This study
20Ni/SiO_2	232.0	29.8	700 °C	[19]
20Ni/ZrO_2	122.0	28.9f	700 °C	[18]
Ni/AlSBA-15	386.0	28.4	700 °C	[20]
NiO/SiO_2	189.3	28.4	800 °C	This study
20Ni/MCM-41	493.0	26.7	700 °C	[19]
20Ni/SBA-16	328.0	21.2	700 °C	[19]
N.C.	N.V.	20.4	500 °C	[8]
N.C.	N.V.	20.0	700 °C	[15]
ReS_2	41.7	19.2	800 °C	This study
N.C.	N.V.	18.7	700 °C	[18]
KIT-6	667.0	18.4	700 °C	[19]
SBA-15	802.0	13.5	700 °C	[19]

Table 3. *Cont.*

Catalyst	SBET (m^2g^{-1})	% H_2 Yield	Temperature	Reference
MCM-41	852.0	11.0	700 °C	[19]
SnO_2	N.V.	7.6	700 °C	[17]
N.C.	N.V.	6.8	800 °C	This study
SBA-16	743.0	5.5	700 °C	[19]
N.C.	N.V.	4.3	700 °C	[22]

Notes. [a]: CI (co-impregnation); [b]: I (impregnation); [c]: S (sol-gel), P (precipitation); N.C., not catalytic; N.V., non-value.

Based on the results of this study, a reaction mechanism explaining H_2 production from catalytic cellulose pyrolysis is proposed (Figure 7). This shows that CH_4 and CO formation is carried out by thermic and catalytic pyrolysis, in contrast to the literature, which mentions that CH_4 is principally obtained through the thermic decomposition of lignin in biomass. Concerning H_2 formation, the H_2 hydrogen production by cellulose pyrolysis is a thermocatalytic process at high temperatures. The% H_2 yield followed the order: Re_3B >> Re_2C > ReB_2 > NiO/SiO_2 > ReS_2 >> T. This behavior is in good agreement with the hydrogen adsorption energies of the catalytic centers (Re > B > Ni >> C > S). These results show that cellulose pyrolysis using rhenium-based catalysts drastically increased H_2 production. In addition, the catalysts benefit the dehydrogenation of H-C-O-H groups to form H_2 instead of cellulose dehydration itself without a catalyst.

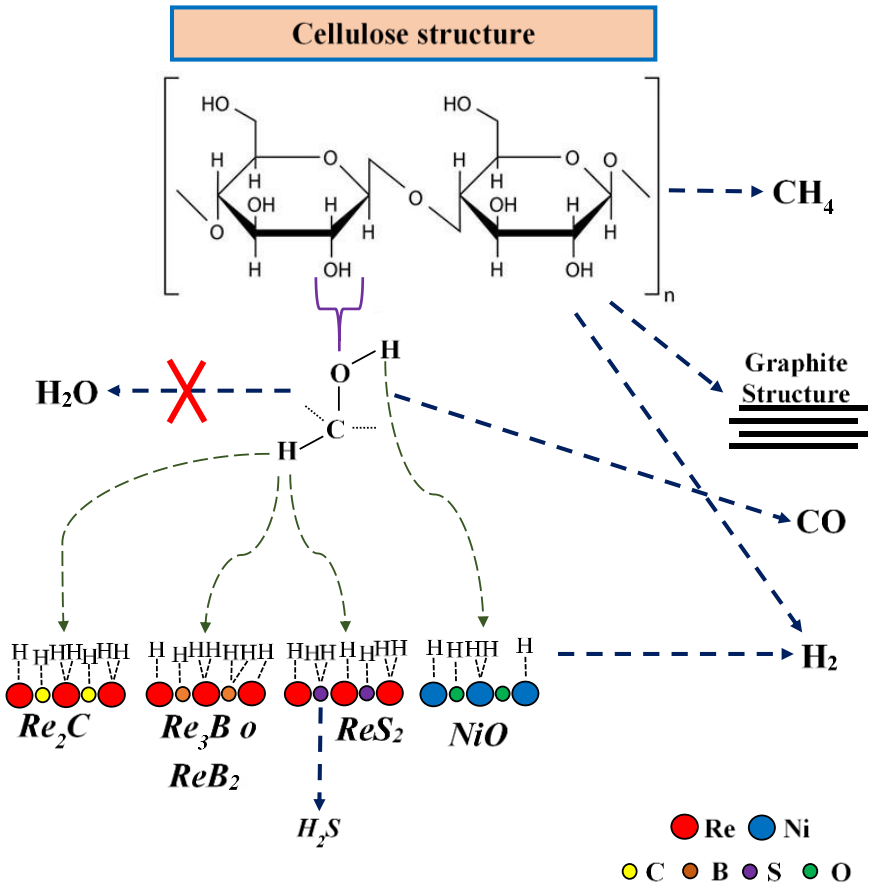


Figure 7. Reaction mechanism for H_2 formation from cellulose pyrolysis using rhenium catalysts.

3.3. Lignin Catalytic Pyrolysis

Similar to the catalytic pyrolysis of cellulose, the results of H_2, CH_4, and CO production, as well as char generation by lignin pyrolysis using rhenium-based catalysts from 500 to 800 °C using 10 and 20 wt.% of catalysts are shown in Figures 8 and 9. The values obtained at 800 °C are listed in Table 4.

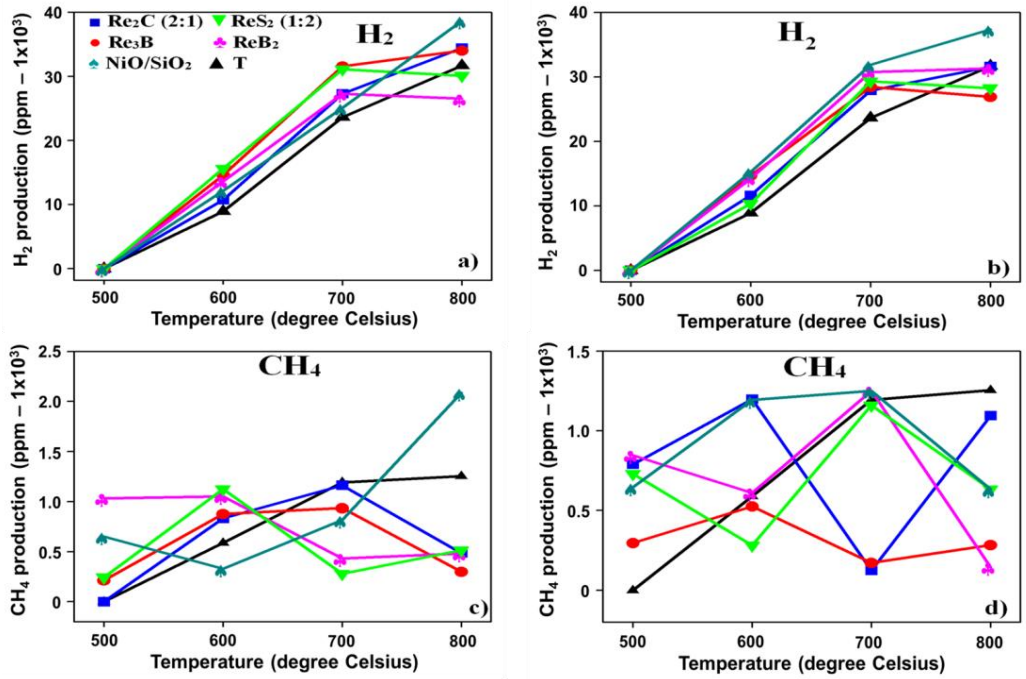


Figure 8. Catalytic pyrolysis of lignin using rhenium catalysts. H_2 production: 10 wt% (**a**) and 20 wt% (**b**); CH_4 production: 10 wt% (**c**) and 20 wt% (**d**).

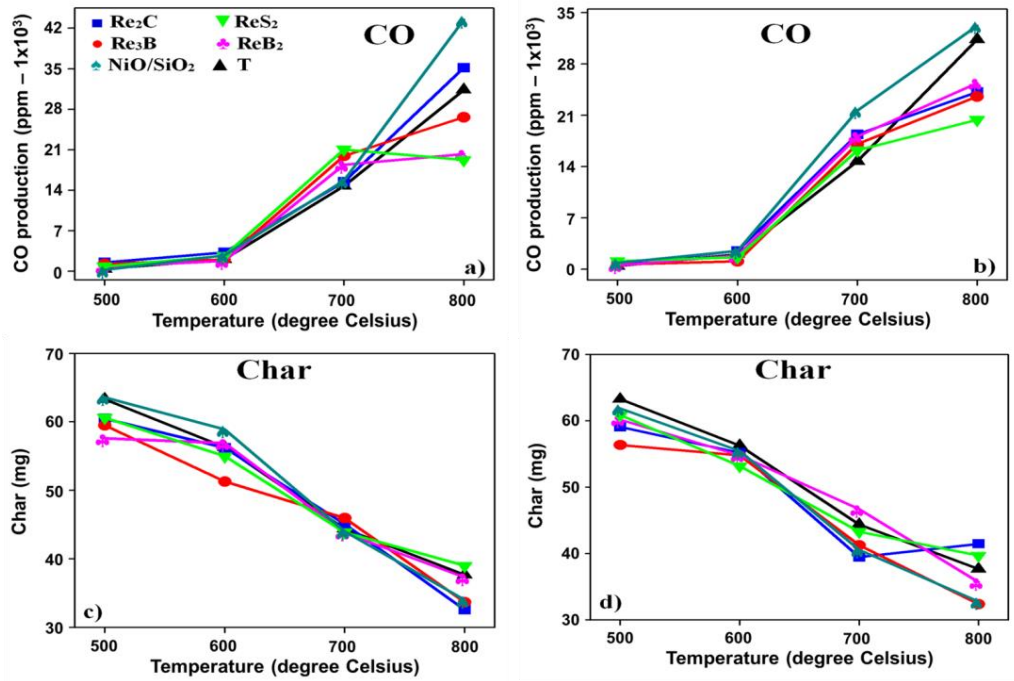


Figure 9. Catalytic pyrolysis of lignin using rhenium catalysts. CO production: 10 wt% (**a**) and 20 wt% (**b**); char generation: 10 wt% (**c**) and 20 wt% (**d**).

Table 4. The production of H_2, CH_4, CO, and char generation during the catalytic pyrolysis of lignin at 800 °C using 10 and 20 wt.% of rhenium-based catalysts.

Catalyst	10 wt.% Catalyst				20 wt.% Catalyst			
	H_2/ppm	CH_4/ppm	CO/ppm	Char/mg	H_2/ppm	CH_4/ppm	CO/ppm	Char/mg
without	31,664	1254	31,347	34.1	31,664	1254	31,347	34.1
ReS_2	30,111	517	19,244	39	28,272	608	20,874	39.4
ReB_2	26,516	481	20,230	37.2	31,324	187	25,640	33.6
Re_3B	34,028	301	26,625	33.9	26,889	294	23,974	32.8
Re_2C	34,399	485	35,182	32.6	31,594	1028	24,961	41.5
NiO/SiO_2	38,687	2089	43,477	33.5	37,393	602	33,281	32.9

Figure 8a shows the H_2 production using 10 wt.% catalyst. The maximum H_2 production was observed using NiO/SiO_2, whereas the minimum was achieved using ReB_2 (Table 4). Increasing the amount of the catalyst to 20 wt.% (Figure 8b), the H_2 production dropped for most of the cases, while just using ReB_2 the production increased slightly. Watanabe et al. [78] reported the H_2 content in lignin is approximately 4.49 wt.% equivalent to 44,900 ppm of H_2. Taking this value as a reference, the H_2 yield achieved from lignin pyrolysis at 800 °C in this study was 59.0% ReB_2 (20 wt.%), 67.7% ReS_2 (10 wt.%), 70.5% without catalyst, 75.7% Re_3B (10 wt.%), 76.6% Re_2C (10 wt.%), and 86.1% NiO/SiO_2 (10 wt.%). The results indicate that only the Re_3B, Re_2C, and NiO/SiO_2 catalysts had a positive effect on H_2 production by lignin pyrolysis using 10 wt.% of the catalyst. However, this increase was not significant, as observed for the production of H_2 by the catalytic pyrolysis of cellulose (Figure 5a). Several studies have been reported on H2 production via lignin pyrolysis under catalytic and non-catalytic conditions. Ferdous et al. [24,25] reported that H_2 formation is the result of breaking lignin subunits and rearranging aromatic rings at high temperatures. Widyawati et al. [27] reported a maximum H_2 production peak at 750 °C. Jung et al. [30] reported an increase in H_2 production at a higher temperature of 500 °C because of the breaking and deformation of C=C and C-H bonds in aromatic rings. Lv et al. [33] reported the catalytic lignin pyrolysis at 700 °C and using nickel and dolomite catalysts found an increase in H_2 production. Collard et al. [34] carried out lignin pyrolysis at 600 °C using Fe and Ni catalysts and found an increase in H_2 production because of the formation of graphitic structure from cracking of aromatic rings attributed to catalysts. Yu et al. [79] reported lignin pyrolysis using dolomite with an increase in H_2 production, while a decrease was observed using a Na_2CO_3 catalyst. These results indicate that H_2 production by lignin during pyrolysis is mainly a thermic process, whereas H_2 production by cellulose pyrolysis is mainly a thermocatalytic process. These results are of great importance because H_2 production by catalytic biomass pyrolysis is only catalytically dependent on the cellulose and hemicellulose fractions and not on the lignin fraction.

The production of CH_4 using 10 wt.% is shown in Figure 8c and the values are in Table 4. These results indicate that all the rhenium-based catalysts explored in this study have a negative effect on CH_4 formation. CH_4 formation is one of the biggest problems in H_2 production from biomass because it involves the reaction of H_2 with carbon. Increasing the amount of catalyst to 20 wt.%, the same trend was observed (Figure 8d). Unusual CH_4 production is a consequence of the complex structure of lignins. This implied that the catalyst did not actively intervene in the formation of H_2 and CH_4 during the catalytic pyrolysis of lignin.

CO production using 10 wt.% of catalysts is shown in Figure 9a and the values are in Table 4. These results indicate that only Re_2C and NiO/SiO_2 had a positive effect on CO

formation. However, when the concentration is increased to 20 wt.% of catalysts (Figure 9b), all rhenium-based catalysts explored show a negative effect on the CO formation. As mentioned above, an increase in CO production indicates an increase in H_2 production. This behavior coincided with the dehydrogenation of aromatic rings [27].

Char generation using 10 wt.% of catalysts is shown in Figure 9c. The maximum char generation was observed using ReS_2, whereas the minimum was achieved using Re_2C (Table 4). Increasing the amount of the catalyst to 20 wt.% (Figure 9d), the maximum char generation was observed using Re_2C, while the minimum was seen using Re_3B. In all cases, the char generation values are within 32.6–41.5 mg, which agrees with the values reported for char generation by lignin pyrolysis (43–44 mg at 800 °C) [24,32].

To compare the results obtained in this study, Table 5 shows the H_2 production by lignin pyrolysis using other methodologies. The H_2 production from steam lignin gasification was omitted because the H_2 yield was overestimated owing to water decomposition. From the information in Table 5, several statements can be made regarding H_2 production by catalytic lignin pyrolysis: (1) the use of catalysts during lignin pyrolysis does not improve H_2 production; (2) the surface area of the catalyst is not a determinant of the% H_2 yield; (3) the% H_2 yield using the NiO/SiO_2 catalyst (86.1%) is the highest reported; and (4) the pyrolysis temperature, up to 800 °C, is the most important parameter for improving% H_2 yield.

Table 5. H_2 yield from pyrolysis of different lignins under non-catalytic and catalytic conditions.

Type of Lignin	Catalyst	SBET (m^2g^{-1})	% H_2 Yield	Temperature	Reference
Alkali lignin	NiO/SiO_2	189.3	86.1	800 °C	This study
Eucalyptus lignin	NiO/H-Y	642.0	81.5	500 °C	[35]
Alkali lignin	Re_2C	0.43	76.6	800 °C	This study
Alkali lignin	Re_3B	0.48	75.7	800 °C	This study
Kraft lignin	N.C.	N.V.	73.0	800 °C	[25]
Alkali lignin	N.C.	N.V.	70.5	800 °C	This study
Alkali lignin	ReS_2	41.7	67.7	800 °C	This study
Eucalyptus lignin	NiO/HSZM-5	330.0	61.4	500 °C	[35]
Eucalyptus lignin	NiO/H-BETA	537.0	61.4	500 °C	[35]
Alkali lignin	ReB_2	0.52	59.0	800 °C	This study
Alkali lignin	N.C.	N.V.	40.0	527 °C	[26]
Dealkaline lignin	N.C.	N.V.	26.3	900 °C	[29]
Merck lignin	N.C.	N.V.	25.8	550 °C	[32]
Alkali lignin	N.C.	N.V.	7.0	500 °C	[8]
Eucalyptus lignin	N.C.	N.V.	6.2	500 °C	[35]

Based on the results observed in this study, a reaction mechanism explaining H_2 production from the catalytic pyrolysis of lignin was proposed (Figure 10). It has been shown that the H_2, CO, and char formation do not require the presence of a rhenium-based catalyst.

Regarding CH_4 formation, the complex structure of lignin and the results obtained from its pyrolysis did not allow us to establish whether this was a catalytic process. However, it can be concluded that H_2 formation via lignin pyrolysis is a thermic process.

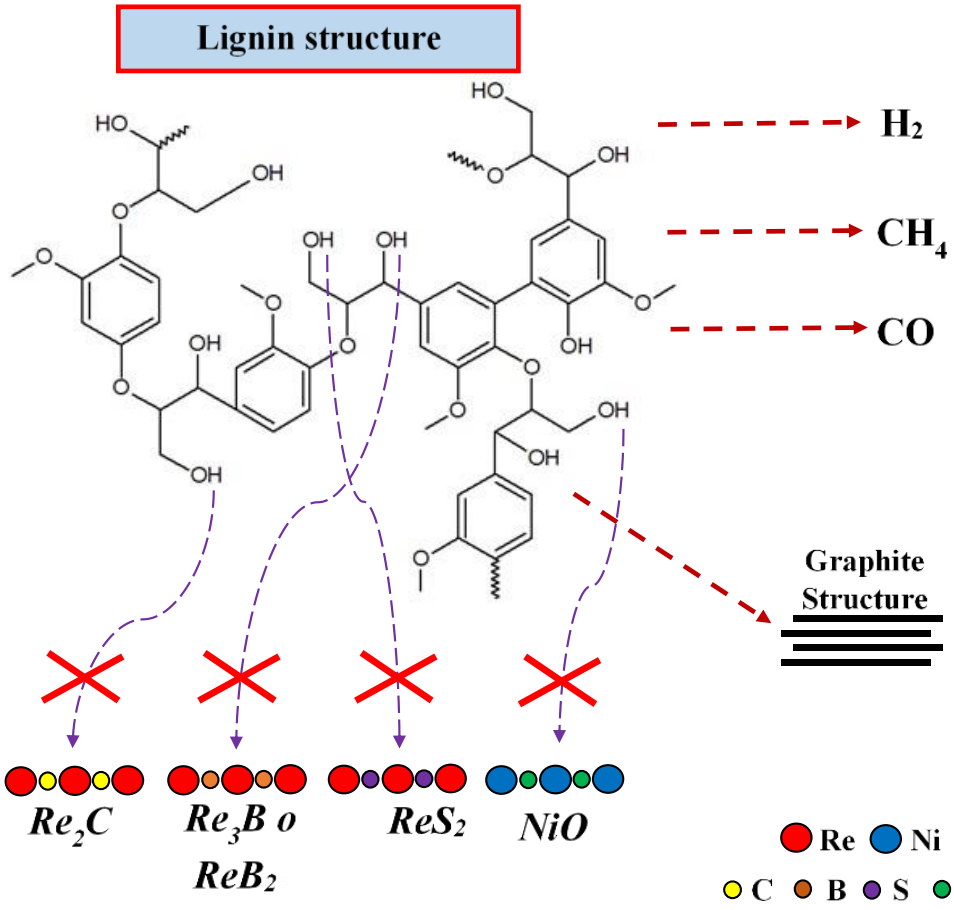


Figure 10. Reaction mechanism for H_2 formation during lignin pyrolysis using rhenium catalysts.

4. Conclusions

In this study, it is reported the use of rhenium-based catalysts for H_2 production via cellulose and lignin pyrolysis. To our knowledge, this is the first report of the mechanosynthesis of ReS_2. Catalytic cellulose pyrolysis results showed the highest H_2 production at 800 °C with 10 wt.% of the Re_3B catalyst. Using the Re_3B catalyst resulted in up to 44% H_2 yield, which is one of the highest reported in the literature. In contrast, ReS_2 had a lower value, which is attributed to the poisoning effect of S on the surface of ReS_2 and the reaction of S and H_2 to form H_2S. H_2 formation by cellulose pyrolysis is a thermocatalytic process, whereas H_2 formation by lignin pyrolysis is an entirely thermic process, in which the use of catalysts does not enhance H_2 production. Therefore, H_2 production by the catalytic pyrolysis of biomass depends only on the cellulose and hemicellulose fractions and not on the lignin fraction.

Supplementary Materials: The following supporting information can be downloaded at: https://www.mdpi.com/article/10.3390/chemistry7020033/s1, Figure S1 Pyrolysis system used in this study; Figure S2 Monitoring system of H_2, CH_4, CO production used in this study.

Author Contributions: Conceptualization, M.G.G.-F., J.M.Q.-M., E.A.J.-A. and M.A.-B.; methodology, M.G.G.-F.; validation, J.M.Q.-M., E.A.J.-A. and M.A.-B.; formal analysis, M.G.G.-F., J.M.Q.-M., E.A.J.-A. and M.A.-B.; investigation, M.G.G.-F.; resources, J.M.Q.-M. and M.A.-B.; data curation, J.M.Q.-M., E.A.J.-A. and M.A.-B.; writing—original draft preparation, M.G.G.-F.; writing—review and editing, J.M.Q.-M., E.A.J.-A. and M.A.-B.; funding acquisition, M.A.-B. All authors have read and agreed to the published version of the manuscript.

Funding: This research was funded by Consejo Nacional de Ciencia y Tecnología (CONACYT), grant number FC-2015-2-947.

Data Availability Statement: Data will be available upon request.

Acknowledgments: This work was supported by the Consejo Nacional de Ciencia y Tecnología (CONACYT) under the grant FC-2015-2-947. The authors wish to acknowledge scholarship support from CONACYT for MGGF. The authors also acknowledge Hector Silva, Beatriz Rivera, Dulce Partida, Gladis Labrada, Ignacio Becerril, Ana Irais Peña, the LINAN, the IPICYT, and the UABC for providing laboratory support.

Conflicts of Interest: The authors declare no conflicts of interest.

References

1. Machrafi, H. *Green Energy and Technology*; Benthan Science Publishers: Sharjah, United Arab Emirates, 2012.
2. Energy Mix. How Much of Global Energy Comes from Low-Carbon Sources. Available online: https://ourworldindata.org/energy-mix (accessed on 11 December 2024).
3. Renewable Energy Market Outlook—2025. Available online: https://www2.deloitte.com/us/en/insights/industry/renewable-energy/renewable-energy-industry-outlook.html (accessed on 11 December 2024).
4. Huggins, R.A. *Energy Storage: Fundamentals, Materials and Applications*, 2nd ed.; Springer: New York, NY, USA, 2015.
5. Gupta, R.B. *Hydrogen Fuel: Production, Transport and Storage*; CRC Press: Boca Raton, FL, USA, 2008.
6. McKendry, P. Energy production from biomass (Part 1): Overview of biomass. *Bioresour. Technol.* **2002**, *83*, 37–46. [CrossRef] [PubMed]
7. Simmons, G.M.; Gentry, M. Kinetic formation of CO, CO_2, H_2, and light hydrocarbon gases from cellulose pyrolysis. *J. Anal. Appl. Pyrolysis* **1986**, *10*, 129–138. [CrossRef]
8. Wu, C.; Wang, Z.; Huang, J.; Williams, P.T. Pyrolysis/gasification of cellulose, hemicellulose and lignin for hydrogen production in the presence of various nickel-based catalysts. *Fuel* **2013**, *106*, 697–706. [CrossRef]
9. Lanza, R.; Nogare, D.D.; Canu, P. Gas phase chemistry in cellulose fast pyrolysis. *Ind. Eng. Chem. Res.* **2009**, *48*, 1391–1399. [CrossRef]
10. Zhao, M.; Yang, X.; Church, T.L.; Harris, A.T. Interaction between a bimetallic Ni-Co catalyst and micrometer-sized CaO for enhanced H_2 production during cellulose decomposition. *Int. J. Hydrogen Energy* **2011**, *36*, 421–431. [CrossRef]
11. Zhao, M.; Yang, X.; Church, T.L.; Harris, A.T. Novel CaO-SiO_2 sorbent and bifunctional Ni/Co-CaO/SiO_2 complex for selective H_2 synthesis from cellulose. *Environ. Sci. Technol.* **2012**, *46*, 2976–2983. [CrossRef]
12. Zhao, M.; Cui, X.; Ji, G.; Zhou, H.; Vuppaladadiyam, A.K.; Zhao, X. Alkaline Thermal Treatment of Cellulosic Biomass for H_2 Production Using Ca-Based Bifunctional Materials. *ACS Sustain. Chem. Eng.* **2019**, *7*, 1202–1209. [CrossRef]
13. Widyaningrum, R.N.; Church, T.L.; Zhao, M.; Harris, A.T. Mesocellular-foam-silica supported Ni catalyst: Effect of pore size on H_2 production from cellulose pyrolysis. *Int. J. Hydrogen Energy* **2012**, *37*, 9590–9601. [CrossRef]
14. Widyaningrum, R.N.; Church, T.L.; Harris, A.T. Promoting effect of Pd on H_2 production from cellulose pyrolysis over mesocellular-foam-supported Ni catalysts. *Catal. Commun.* **2013**, *35*, 45–50. [CrossRef]
15. Matras, J.; Niewiadomski, M.; Ruppert, A.; Grams, J. Activity of Ni catalysts for hydrogen production via biomass pyrolysis. *Kinet. Catal.* **2012**, *53*, 565–569. [CrossRef]
16. Ruppert, A.M.; Niewiadomski, M.; Grams, J.; Kwapiński, W. Optimization of Ni/ZrO_2 catalytic performance in thermochemical cellulose conversion for enhanced hydrogen production. *Appl. Catal. B Environ.* **2014**, *145*, 85–90. [CrossRef]
17. Donar, Y.O.; Sinağ, A. Catalytic effect of tin oxide nanoparticles on cellulose pyrolysis. *J. Anal. Appl. Pyrolysis* **2016**, *119*, 69–74. [CrossRef]
18. Grams, J.; Niewiadomski, M.; Ryczkowski, R.; Ruppert, A.M.; Kwapiński, W. Activity and characterization of Ni catalyst supported on CeO_2-ZrO_2 for thermo-chemical conversion of cellulose. *Int. J. Hydrogen Energy* **2016**, *41*, 8679–8687. [CrossRef]
19. Grams, J.; Potrzebowska, N.; Goscianska, J.; Michalkiewicz, B.; Ruppert, A.M. Mesoporous silicas as supports for Ni catalyst used in cellulose conversion to hydrogen rich gas. *Int. J. Hydrogen Energy* **2016**, *41*, 8656–8667. [CrossRef]
20. Grams, J.; Goscianska, J.; Potrzebowska, N.; Ryczkowski, R.; Michalkiewicz, B.; Ruppert, A.M. Impact of Zr Incorporation into the Ni/AlSBA-15 Catalyst on Its Activity in Cellulose Conversion to Hydrogen-Rich Gas. *Energy Fuels* **2017**, *31*, 14089–14096. [CrossRef]
21. Ryczkowski, R.; Niewiadomski, M.; Michalkiewicz, B.; Skiba, E.; Ruppert, A.M.; Grams, J. Effect of alkali and alkaline earth metals addition on Ni/ZrO_2 catalyst activity in cellulose conversion. *J. Therm. Anal. Calorim.* **2016**, *126*, 103–110. [CrossRef]
22. Ryczkowski, R.; Ruppert, A.M.; Przybysz, P.; Chałupka, K.; Grams, J. Hydrogen production from biomass woodchips using Ni/CaO–ZrO_2 catalysts. *React. Kinet. Mech. Catal.* **2017**, *121*, 97–107. [CrossRef]

23. Memon, M.Z.; Ji, G.; Li, J.; Zhao, M. Na_2ZrO_3 as an Effective Bifunctional Catalyst Sorbent during Cellulose Pyrolysis. *Ind. Eng. Chem. Res.* **2017**, *56*, 3223–3230. [CrossRef]
24. Ferdous, D.; Dalai, A.K.; Bej, S.K.; Thring, R.W.; Bakhshi, N.N. Production of H_2 and medium Btu gas via pyrolysis of lignins in a fixed-bed reactor. *Fuel Process. Technol.* **2001**, *70*, 9–26. [CrossRef]
25. Ferdous, D.; Dalai, A.K.; Bej, S.K.; Thring, R.W. Pyrolysis of lignins: Experimental and kinetics studies. *Energy Fuels* **2002**, *16*, 1405–1412. [CrossRef]
26. Baumlin, S.; Broust, F.; Bachi, F.B.; Bourdeaux, T.; Herbinet, O.; Ndiaye, F.T.; Ferrer, M.; Lédé, J. Production of hydrogen by lignins fast pyrolysis. *Int. J. Hydrogen Energy* **2006**, *31*, 2179–2192. [CrossRef]
27. Widyawati, M.; Church, T.L.; Florin, N.H.; Harris, A.T. Hydrogen synthesis from biomass pyrolysis with in situ carbon dioxide capture using calcium oxide. *Int. J. Hydrogen Energy* **2011**, *36*, 4800–4813. [CrossRef]
28. Trinh, T.N.; Jensen, P.A.; Sárossy, Z.; Johansen, K.D.; Knudsen, N.O.; Sørensen, H.R.; Egsgaard, H. Fast pyrolysis of lignin using a pyrolysis centrifuge reactor. *Energy Fuels* **2013**, *27*, 3802–3810. [CrossRef]
29. Zhou, H.; Wu, C.; Onwudili, J.A.; Meng, A.; Zhang, Y.; Williams, P.T. Polycyclic aromatic hydrocarbon formation from the pyrolysis/gasification of lignin at different reaction conditions. *Energy Fuels* **2014**, *28*, 6371–6379. [CrossRef]
30. Jung, K.A.; Nam, C.W.; Woo, S.H.; Park, J.M. Response surface method for optimization of phenolic compounds production by lignin pyrolysis. *J. Anal. Appl. Pyrolysis* **2016**, *120*, 409–415. [CrossRef]
31. Volpe, R.; Zabaniotou, A.A.; Skoulou, V. Synergistic Effects between Lignin and Cellulose during Pyrolysis of Agricultural Waste. *Energy Fuels* **2018**, *32*, 8420–8430. [CrossRef]
32. Akubo, K.; Nahil, M.A.; Williams, P.T. Pyrolysis-catalytic steam reforming of agricultural biomass wastes and biomass components for production of hydrogen/syngas. *J. Energy Inst.* **2019**, *92*, 1987–1996. [CrossRef]
33. Lv, P.; Chang, J.; Wang, T.; Wu, C.; Tsubaki, N. A kinetic study on biomass fast catalytic pyrolysis. *Energy Fuels* **2004**, *18*, 1865–1869. [CrossRef]
34. Collard, F.X.; Blin, J.; Bensakhria, A.; Valette, J. Influence of impregnated metal on the pyrolysis conversion of biomass constituents. *J. Anal. Appl. Pyrolysis* **2012**, *95*, 213–226. [CrossRef]
35. Milovanović, J.; Luque, R.; Tschentscher, R.; Romero, A.A.; Li, H.; Shih, K.; Rajić, N. Study on the pyrolysis products of two different hardwood lignins in the presence of NiO contained-zeolites. *Biomass Bioenergy* **2017**, *103*, 29–34. [CrossRef]
36. Yang, H.; Norinaga, K.; Li, J.; Zhu, W.; Wang, H. Effects of HZSM-5 on volatile products obtained from the fast pyrolysis of lignin and model compounds. *Fuel Process. Technol.* **2018**, *181*, 207–214. [CrossRef]
37. Simonetti, D.A.; Kunkes, E.L.; Dumesic, J.A. Gas-phase conversion of glycerol to synthesis gas over carbon-supported platinum and platinum-rhenium catalysts. *J. Catal.* **2007**, *247*, 298–306. [CrossRef]
38. Granados-Fitch, M.G.; Quintana-Melgoza, J.M.; Juarez-Arellano, E.A.; Avalos-Borja, M. Mechanism to H_2 production on rhenium carbide from pyrolysis of coconut shell. *Int. J. Hydrogen Energy* **2019**, *44*, 2784–2796. [CrossRef]
39. Granados-Fitch, M.G.; Quintana-Melgoza, J.M.; Juarez-Arellano, E.A.; Avalos-Borja, M. Rhenium borides (Re_3B and ReB_2) mechanosynthesis and their use as a catalyst for H_2 production from biomass pyrolysis. *Mater. Res. Bull.* **2021**, *137*, 111180. [CrossRef]
40. Granados-Fitch, M.G.; Juarez-Arellano, E.A.; Quintana-Melgoza, J.M.; Avalos-Borja, M. Mechanosynthesis of rhenium carbide at ambient pressure and temperature. *Int. J. Refract. Met. Hard Mat.* **2016**, *55*, 11–15. [CrossRef]
41. Granados-Fitch, M.G.; Quintana-Melgoza, J.M.; Juarez-Arellano, E.A.; Avalos-Borja, M. Chemical stability of ReB_2 at oxygen and moisture ambient environmental conditions prepared by mechanical milling. *J. Am. Ceram. Soc.* **2018**, *101*, 3148–3155. [CrossRef]
42. Murray, H.H.; Kelty, S.P.; Chianelli, R.R.; Day, C.S. Structure of Rhenium Disulfide. *Inorg. Chem.* **1994**, *33*, 4418–4420. [CrossRef]
43. Coleman, K.S.; Sloan, J.; Hanson, N.A.; Brown, G.; Clancy, G.P.; Terrones, M.; Terrones, H.; Green, M.L.H. The Formation of ReS_2 Inorganic Fullerene-like Structures Containing Re_4 Parallelogram Units and Metal–Metal Bonds. *Am. Chem. Soc.* **2002**, *124*, 11580–11581. [CrossRef]
44. Yella, A.; Therese, H.A.; Zink, N.; Panthöfer, M.; Tremel, W. Large Scale MOCVD Synthesis of Hollow ReS_2 Nanoparticles with Nested Fullerene-Like Structure. *Chem. Mater.* **2008**, *20*, 3587–3593. [CrossRef]
45. Ho, T.C.; Shen, Q.; McConnachie, J.M.; Kliewer, C.E. Kinetic characterization of unsupported ReS_2 as hydroprocessing catalyst. *J. Catal.* **2010**, *176*, 114–122. [CrossRef]
46. Tu, W.; Denizot, B. Synthesis of small-sized rhenium sulfide colloidal nanoparticles. *J. Colloid Interface Sci.* **2007**, *30*, 167–170. [CrossRef] [PubMed]
47. Uvarov, V.; Popov, I. Metrological characterization of X-ray diffraction methods for determination of crystallite size in nano-scale materials. *Mater. Charact.* **2007**, *58*, 883–891. [CrossRef]
48. Garnier, G.; Bouchard, J.; Overend, R.P.; Chornet, E.; Vidal, P.F. High yield production of microcrystalline cellulose by a thermo-mechano-solvolytic treatment. *Can. J. Chem. Eng.* **1990**, *68*, 113–118. [CrossRef]
49. Che, M. Nobel Prize in chemistry 1912 to Sabatier: Organic chemistry or catalysis? *Catal. Today* **2013**, *218–219*, 162–171. [CrossRef]

50. Ferro, Y.; Marinelli, F.; Allouche, A.; Brosset, C. Density functional theory investigation of H adsorption on the basal plane of boron-doped graphite. *J. Chem. Phys.* **2003**, *118*, 5650–5657. [CrossRef]
51. Ferro, Y.; Marinelli, F.; Jelea, A.; Allouche, A. Adsorption, diffusion, and recombination of hydrogen on pure and boron-doped graphite surfaces. *J. Chem. Phys.* **2004**, *120*, 11882–11888. [CrossRef]
52. Dowling, N.I.; Hyne, J.B.; Brown, D.M.; Brown, D.M. Kinetics of the Reaction between Hydrogen and Sulfur under High-Temperature Claus Furnace Conditions. *Ind. Eng. Chem. Res.* **1990**, *29*, 2327–2332. [CrossRef]
53. Ducros, R.; Ehrhardt, J.J.; Alnot, M.; Cassuto, A. Hydrogen and deuterium adsorption on polycrystalline rhenium surfaces; effect of carbon and oxygen coadsorption. *Surf. Sci.* **1976**, *55*, 509–522. [CrossRef]
54. Pallassana, V.; Neurock, M. Theoretical analysis of hydrogen chemisorption on Pd(111), Re(0001) and PdML/Re(0001), ReML/Pd(111) pseudomorphic overlayers. *Phys. Rev. B Condens. Matter Mater. Phys.* **1999**, *60*, 6146–6154. [CrossRef]
55. Poulter, K.F.; Pryde, J.A. Chemisorption of hydrogen on rhenium. *J. Phys. D. Appl. Phys.* **1968**, *1*, 169–172. [CrossRef]
56. Muschiol, U.; Lenz, J.; Schwarz, E.; Christmann, K. Interaction of hydrogen with Re(10 10): H binding states and ordered phases. *Surf. Sci.* **1995**, *333*, 127–132. [CrossRef]
57. Zhou, Z.; Zhao, J.; Chen, Z.; Gao, X.; Yan, T.; Wen, B.; Schleyer, P.V.R. Comparative study of hydrogen adsorption on carbon and BN nanotubes. *J. Phys. Chem. B* **2006**, *110*, 13363–13369. [CrossRef] [PubMed]
58. Shao, X.; Luo, H.; Cai, J.; Dong, C. First-principles study of single atom adsorption on capped single-walled carbon nanotubes. *Int. J. Hydrogen Energy* **2014**, *39*, 10161–10168. [CrossRef]
59. Andreoni, W.; Curioni, A.; Kroes, J.M.H.; Pietrucci, F.; Gröning, O. Exohedral hydrogen chemisorption on a carbon nanotube: The clustering effect. *J. Phys. Chem. C* **2012**, *116*, 269–275. [CrossRef]
60. Kayanuma, M.; Nagashima, U.; Nishihara, H.; Kyotani, T.; Ogawa, H. Adsorption and diffusion of atomic hydrogen on a curved surface of microporous carbon: A theoretical study. *Chem. Phys. Lett.* **2010**, *495*, 251–255. [CrossRef]
61. Boukhvalov, D.W.; Katsnelson, M.I.; Lichtenstein, A.I. Hydrogen on graphene: Electronic structure, total energy, structural distortions and magnetism from first-principles calculations. *Phys. Rev. B Condens. Matter Mater. Phys.* **2008**, *77*, 035427. [CrossRef]
62. Yang, M.; Nurbawono, A.; Zhang, C.; Wu, R.; Feng, Y. Ariando, Manipulating absorption and diffusion of H atom on graphene by mechanical strain. *AIP Adv.* **2011**, *1*, 032109. [CrossRef]
63. Casolo, S.; Løvvik, O.M.; Martinazzo, R.; Tantardini, G.F. Understanding adsorption of hydrogen atoms on graphene. *J. Chem. Phys.* **2009**, *130*, 054704. [CrossRef]
64. Katin, K.P.; Prudkovskiy, V.S.; Maslov, M.M. Chemisorption of hydrogen atoms and hydroxyl groups on stretched graphene: A coupled QM/QM study. *Phys. Lett. A* **2017**, *381*, 2686–2690. [CrossRef]
65. Radosinski, L.; Kuchta, B. Hydrogen chemisorption on carbon structure with mixed sp2 sp3 hybridization: Empirical potential studies. *Adsorption* **2014**, *20*, 875–882. [CrossRef]
66. Mårlid, B.; Larsson, K.; Carlsson, J.O. Chemical interaction of H_2, Br_2, and HBr with α boron surfaces. *J. Phys. Chem. B* **2001**, *105*, 12797–12802. [CrossRef]
67. Oku, T. Hydrogen storage in boron nitride and carbon nanomaterials. *Energies* **2015**, *8*, 319–337. [CrossRef]
68. Koi, N.; Oku, T. Molecular orbital calculations of hydrogen storage in carbon and boron nitride clusters. *Sci. Technol. Adv. Mater.* **2004**, *5*, 625–628. [CrossRef]
69. Manchanda, P.; Enders, A.; Sellmyer, D.J.; Skomski, R. Hydrogen-induced ferromagnetism in two-dimensional Pt dichalcogenides. *Phys. Rev. B* **2016**, *94*, 104426. [CrossRef]
70. Chen, W.; Santos, E.J.G.; Zhu, W.; Kaxiras, E.; Zhang, Z. Tuning the electronic and chemical properties of monolayer MoS_2 adsorbed on transition metal substrates. *Nano Lett.* **2013**, *13*, 509–514. [CrossRef] [PubMed]
71. Han, S.W.; Cha, G.B.; Park, Y.; Hong, S.C. Hydrogen physisorption based on the dissociative hydrogen chemisorption at the sulfur vacancy of MoS_2 surface. *Sci. Rep.* **2017**, *7*, 7152. [CrossRef]
72. Mele, F.; Russo, N.; Toscano, M. Hydrogen chemisorption on the Ni(100) surface: Electronic and magnetic properties from a local-spin-density study. *Surf. Sci.* **1991**, *251–252*, 46–50. [CrossRef]
73. Paul, J.F.; Sautet, P. Comparison of the nature of the hydrogen-metal bond on Pd(111) and Ni(111) by a periodic density functional method. *Surf. Sci.* **1996**, *356*, L403–L409. [CrossRef]
74. Klinke, D.J.; Dooling, D.J.; Broadbelt, L.J. Theoretical study of methylidyne chemisorption on Ni(111) and Co(0001) surfaces. *Surf. Sci.* **1999**, *425*, 334–342. [CrossRef]
75. Yeo, J.Y.; Chin, B.L.F.; Tan, J.K.; Loh, Y.S. Comparative studies on the pyrolysis of cellulose, hemicellulose, and lignin based on combined kinetics. *J. Energy Inst.* **2019**, *92*, 27–37. [CrossRef]
76. Ferreiro, A.I.; Rabaçal, M.; Costa, M.; Giudicianni, P.; Grottola, C.M.; Ragucci, R. Modeling the impact of the presence of KCl on the slow pyrolysis of cellulose. *Fuel* **2018**, *215*, 57–65. [CrossRef]
77. Wang, W.; Shi, Y.; Cui, Y.; Li, X. Catalytic fast pyrolysis of cellulose for increasing contents of furans and aromatics in biofuel production. *J. Anal. Appl. Pyrolysis* **2018**, *131*, 93–100. [CrossRef]

78. Watanabe, H.; Shimomura, K.; Okazaki, K. Carbonate formation during lignin pyrolysis under CO_2 and its effect on char oxidation. *Proc. Combust. Inst.* **2015**, *35*, 2423–2430. [CrossRef]
79. Yu, H.; Wu, Z.; Chen, G. Catalytic gasification characteristics of cellulose, hemicellulose and lignin. *Renew. Energy* **2018**, *121*, 559–567. [CrossRef]

Disclaimer/Publisher's Note: The statements, opinions and data contained in all publications are solely those of the individual author(s) and contributor(s) and not of MDPI and/or the editor(s). MDPI and/or the editor(s) disclaim responsibility for any injury to people or property resulting from any ideas, methods, instructions or products referred to in the content.